

Title No. 116-M86

Extension of Powers-Brownyard Model to Pastes Containing Supplementary Cementitious Materials

by Deborah Glosser, Vahid Jafari Azad, Prannoy Suraneni, O. Burkan Isgor, and W. Jason Weiss

The properties of cementitious materials depend on the proportions of unhydrated phases, hydrated phases, and pore volumes in the paste. The Powers-Brownyard model (PB model) has been used to estimate these volumes for ordinary portland cement (OPC) as a function of degree of hydration. However, the PB model was not developed for systems containing supplementary cementitious materials (SCMs). This work combines the PB model and thermodynamic calculations to predict capillary and gel porosity, chemical shrinkage, and the volumes of all hydrated and unhydrated phases for OPC-SCM pastes. SCM reactivity is a dominant factor in predicting the hydrated paste phase and pore volumes in OPC-SCM systems. Pore refinement occurs with increasing SCM reactivity, and the proportion of gel pores relative to solids increases from Powers-Brownyard assumptions when SCM is used. The proposed model provides additional information on unreacted and reacted phase volumes.

Keywords: porosity; Powers-Brownyard model; supplementary cementitious material (SCM); thermodynamic modeling.

INTRODUCTION

Replacement of ordinary portland cement (OPC) by supplementary cementitious materials (SCMs) in concrete provides a host of environmental, economic, and performance benefits.^{1,2} Powers and Brownyard developed a model to predict the volume of hydrated products.³ However, this model was limited to OPC and does not apply to OPC-SCM systems.⁴⁻⁸

The Powers-Brownyard model (PB model) is a relatively simple, yet powerful tool that can be used to determine the volumetric relationships between unhydrated cement, water, and the hydrated products of cement as a function of cement hydration³. The PB model has been used to predict properties of concrete including strength,⁹ freezing-and-thawing resistance,¹⁰ shrinkage and creep,¹¹ and transport.¹² However, the PB model does not provide information on the exact hydrated solid phase compositions, pore solution composition, or pore solution alkalinity.¹¹ Further, the PB model is generally limited to OPC systems, although there have been prior attempts to apply it to SCMs.¹³⁻¹⁵

It has been previously shown that the PB model can be coupled with thermodynamic calculations and kinetic models for OPC pastes to overcome some of these described limitations.¹¹ Thermodynamic modeling can predict the volumes of unhydrated and hydrated solid phases and ionic concentrations in pore solutions of cementitious systems. On the other hand, the PB model can describe the volumes of different pores in the system (that is, gel and capillary water contents). Therefore, there is significant benefit of this coupling approach to provide more comprehensive infor-

mation about the hydrated products and pore structure of a wide variety of cementitious systems. However, OPC-SCM pastes present additional challenges when compared to systems that only contain OPC binder. While it is established that SCMs react more slowly than OPC, the precise degree of reactivity (DoR) of an SCM is not easily obtained experimentally,¹⁵ and there are presently no analytical models to accurately predict it.^{16,17}

The present work demonstrates a method to extend the PB model with thermodynamic calculations to interpret pore volumes and predict detailed hydrated and unhydrated phase volumes in OPC-SCM systems. The model presented in this paper (the “pore partitioning model”) addresses the reactivity-related challenges of the OPC-SCM systems by treating cement degree of hydration (DoH) and SCM DoR separately and by providing simulations for a range of SCM DoR. The model provides information to clarify and separate the effects of SCM replacement volume, SCM reactivity, and chemical composition of the binder on resulting phase assemblages and porosity in OPC-SCM systems as a function of DoH. This information can be used to both aid in the design of OPC-equivalent mixtures and in the selection of SCMs based on the salient factors driving the evolution of the paste properties, rather than relying solely on binder chemical composition.

RESEARCH SIGNIFICANCE

This work extends the work of Powers-Brownyard using thermodynamic calculations to predict capillary and gel porosity, chemical shrinkage, and volumes of hydrated and unhydrated phases for OPC-SCM systems. The present model fills a critical knowledge gap by combining thermodynamic principles with established cement kinetics to provide detailed pore and phase volume data that can potentially be used to design pastes that are optimized for properties such as strength, freezing-and-thawing resistance, shrinkage, and creep. This data could be used to elucidate structure/property relations of hardened concrete, and to model transport properties of concrete produced with SCMs, much like the PB model does.

ACI Materials Journal, V. 116, No. 5, September 2019.

MS No. M-2018-272, doi: 10.14359/51714466, received July 17, 2018, and reviewed under Institute publication policies. Copyright © 2019, American Concrete Institute. All rights reserved, including the making of copies unless permission is obtained from the copyright proprietors. Pertinent discussion including author's closure, if any, will be published ten months from this journal's date if the discussion is received within four months of the paper's print publication.

MODELING APPROACH

The following sections describe the background for the models used in the pore partitioning model. The theoretical foundation of this model includes the PB model, OPC hydration kinetics, SCM degrees of reactivity, and thermodynamic modeling.

PB model

The classic PB model³ enables the computation of phase volumes. Specifically, this includes unhydrated cement volume (V_c), gel solids (V_{gs}), gel water (V_{gw}), capillary water (V_{cw}), and chemical shrinkage (V_{cs}). The PB model assumes that the phase volume amounts are linearly related to the DoH, and that the gel water is 19% of the gel solids. A salient feature of the PB model is that ultimately all predicted volumes depend only on the water-cement ratio (w/c) and porosity. The model is discussed at length in prior works.^{9,18,19} The normalized phase volumes are calculated in the pore partitioning model using the PB model. The PB model is defined by the following equations

$$V_c = (1 - p)(1 - \alpha) \quad (1a)$$

$$V_{gs} = (1 - 6.4 \times 10^{-5}) \rho_c + 0.23 \frac{\rho_c}{\rho_w} (1 - p) \alpha \quad (1b)$$

$$V_{gw} = 0.19 \frac{\rho_c}{\rho_w} (1 - p) \alpha \quad (1c)$$

$$V_{cw} = p - 0.42 \frac{\rho_c}{\rho_w} (1 - p) \alpha \quad (1d)$$

$$V_{cs} = 6.4 \times 10^{-5} \rho_c (1 - p) \alpha \quad (1e)$$

$$p = \frac{w/c}{w/c + \frac{\rho_c}{\rho_w}} \quad (1f)$$

where p is the volume fraction of initial porosity of the paste; α is degree of hydration (%); w/c is the water-cement ratio (kg/kg or lb/lb); ρ_c , ρ_w are the densities of cement and density of water (kg/m³ or lb/in.³), respectively. In the PB model, the gel water content (g/g or in.³/in.³) is approximately 0.19 g/g (or 0.60 in.³/in.³) of reacted cement.

OPC hydration kinetics

The Parrot and Killoh model^{20,21} is used to account for the hydration kinetics of OPC. The pore partitioning model uses the Parrot and Killoh model to calculate the dissolution rate and DoH of major cement phases. The Parrot and Killoh model was developed for OPC and is not applicable for SCM-blended systems. Therefore, it was used to determine the ratios of the dissolved cement phases only.

The Parrot and Killoh model describes cement hydration as a diffusion-controlled process, where the rate is constrained by the slowest clinker phase hydration rate at

time t . This rate then controls the nucleation, growth, and ultimately diffusion processes

$$\alpha_{ph}(t) = \int_0^t \left(\min \left\{ \frac{A}{A_0} r_{ph,i} r_{ph,2} r_{ph,3} \right\} f_{w/b} \beta_H e^{\left(\frac{E_i}{R} \left(\frac{1}{T_0} - \frac{1}{T} \right) \right)} \right) dt \quad (2a)$$

where $\alpha_{ph}(t)$ is the degree of hydration of each phase at time t (days); $r_{ph,i}$ ($i = 1, 2, 3$) is the dissolution rate of each phase due to nucleation (Eq. (2b)), diffusion (Eq. (2c)), and growth (Eq. (2d)); $f_{w/b}$ is a function to account for the effects of water-binder ratio (w/b), based on the total degree of hydration of the system as a weighted average of all phases; β_H is an empirical parameter that accounts for the effects of relative humidity; A is the Blaine surface area (m²/kg [ft²/lb]), A_0 is the reference Blaine surface area (385 m²/kg [1879.7 ft²/lb]); E_i is the activation energy for cement phase dissolution rates (J/mol or btu/mol); R is the universal gas constant (8.314 J/mol·K [4.38 × 10⁻³ btu/mol·°F]); T_0 is the reference temperature (298.15 K [77°F]), and T is the temperature at which the analysis is performed. Ultimately, the Parrot-Killoh model accounts for the time dependent kinetics in OPC. The rates of dissolution are calculated as follows

$$r_{ph,1} = \frac{K_{ph,1}}{N_{ph,1}} (1 - \alpha_{ph}(t)) (-\ln(1 - \alpha_{ph}(t)))^{1 - N_{ph,1}} \quad (3a)$$

$$r_{ph,2} = \frac{K_{ph,2} \sqrt[3]{(1 - \alpha_{ph}(t))^2}}{1 - \sqrt[3]{(1 - \alpha_{ph}(t))}} \quad (3b)$$

$$r_{ph,3} = K_{ph,3} (1 - \alpha_{ph}(t))^{N_{ph,3}} \quad (3c)$$

where $K_{ph,i}$ and $N_{ph,i}$ ($i = 1, 2, 3$) were defined by the Parrot and Killoh model and later refined by Lothenbach et al.^{21,22} These rates are dependent on the degree of hydration of each phase in the cement paste. The dissolution of other oxides (for example, Na₂O) are modeled proportionally with DoH.

Thermodynamic model

Thermodynamic modeling is used in the pore partitioning model to independently predict phase composition and chemical shrinkage of OPC-SCM pastes. Thermodynamic calculations are performed using GEMS3K,²³ which is an open-source software based on the Gibbs free energy minimization technique. The CEMDATA (Version 14.01) thermodynamic database is used in this work,^{21,22,24-34} and the high volumes of thermodynamic computations were performed with the aid of a Java program developed by the authors to automate the GEMS3K calculations and the Parrot and Killoh OPC kinetics calculations. GEMS3K simultaneously computes the molar amounts of dependent components (molecules and ions), their activities, and the chemical potentials of the system. The software output includes information on all stable solid, aqueous, and gas phases. The Gibbs energy minimization algorithm employed by GEMS3K first calculates the molar Gibbs free energy of each of the components in the OPC and SCM as a function

of pressure and temperature. The equilibrium state at that pressure and temperature is then determined by the global minimum of the total system's Gibbs energy. In this way, the software determines the unknown phase assemblages and speciation of phases produced by the OPC and SCM reactions by minimizing the total Gibbs energy of the system, while maintaining the system mass balance. Detailed descriptions of GEMS3K-CEM DATA and the Gibbs energy minimization technique are presented in other works.^{23,35}

Pore partitioning model

The pore partitioning model synthesizes the approaches described in Sections 3.1 through 3.3 to model detailed phase volumes, porosity, and pore solution chemistry in OPC-SCM systems. The main assumptions and the steps of the model are described in the following.

Assumptions and modeling process—Dissolution rates of the OPC phases and DoH are calculated using the Parrott-Killoh model. However, because no widely accepted empirical model to describe SCM kinetics exists, the pore partitioning model assumes a uniform dissolution for SCM oxides. In other words, the same DoR is applied to all oxides of a given SCM, which is an assumption that can be improved in future work as more information on SCM and cement oxide dissolution rates becomes available.^{36,37} For purposes of this model, a wide range of SCM DoRs were simulated to capture the variability in composition, particle size, crystallinity, and other factors that are known to cause variations in the reactivity of SCM.

Thermodynamic modeling is then performed using GEMS3K to calculate phase volumes and assemblages, as well as the total amount of water released from major phases at each degree hydration. The pore partitioning model blocks hydrogarnet phases from the output because these phases do not form at standard temperature and pressure in OPC systems during typical service life periods.¹¹ As a result, it is also assumed that these phases will not form in blended systems. Due to the limited early-age reactivity of SCMs and imprecise kinetics rules for these systems, early ages (that is, DoH < 30%) are not modeled.

At each step in the analysis where the *w/b*, DoH, and DoR are fixed, thermodynamic calculations are performed using GEMS3K, which independently computes the hydrated phase volumes (solid and aqueous), as well as pore solution composition, at any given stage of hydration.

Gel water calculations—The thermodynamic modeling cannot independently distinguish between gel water and capillary water but it does provide the amount of water that remains in each system following hydration and reaction. It also provides the amount of water that is chemically bound to each phase following reaction. Although there is no distinction between gel and capillary water in the thermodynamic calculation itself, it is known that only certain hydrated solid phases will contain gel water.¹¹

The pore partitioning model computes gel water (the liquid water/pore solution contained in gel pores) as being comprised of two parts: the water that is released by major phases upon heating to 100°C (ettringite, monosulfate, hydroalcalite), and the portion of water that remains in small

pores of the hydrated product (that is, “gel”) following hydration and reaction. Gel water calculation is a multistep process that follows the following steps:

1. The calculation of released water from the major phases using¹¹

$$V_{w, released} = \sum_{i=1}^{n, ph} \frac{n_i H_{i, ph} V_{H_2O}}{V_{t, init}} \quad (4a)$$

where $V_{w, released}$ is the normalized released water volume from all phases (m^3/m^3 or ft^3/ft^3); i is the index corresponding to a particular phase; n, ph is the number of phases; n_i is the number of moles of the respective phase, $H_{i, ph}$ is the number of water molecules in each phase; and V_{H_2O} is the molar volume of water ($18.015 \times 10^{-6} m^3/mol$ [$632.2 \times 10^{-6} ft^3/mol$]); and $V_{t, init}$ is the total volume of the initial system (m^3), including water and unhydrated and unreacted material. The phases which release water are ettringite, monosulfate, and, when present, hydrogarnet and hydroalcalite. The “release” of water occurs when the cement is dried to 0% humidity. Because the high temperatures that result from hydration reactions can cause these phases to lose water when at a relative humidity of $\leq 80\%$, it is assumed for purposes of this calculation that all of the water bound to these phases is released.

The total volume of gel water in the system will be related to the total volume of C-S-H in the system. For that reason, total C-S-H volumes are calculated as follows

2. The calculation of total C-S-H volumes

$$V_{C-S-H} = \frac{\sum_{i=1}^4 n_i (v_{C-S-H})_i}{v_{t, init}} \quad (4b)$$

where V_{C-S-H} is the normalized volume of total C-S-H in the system (m^3/m^3 [ft^3/ft^3]) which, according to the thermodynamic database (CEM DATA), is comprised of the following four variants: Jennite (Types D and H) and Tobermorite (Types D and H) based on calcium-to-silica ratio (*C/S*); n is the number of moles of variant i C-S-H (m^3/m^3 [ft^3/ft^3]); $(V_{C-S-H})_{ni}$ is the molar volume of type n , C-S-H; and i is the variant of C-S-H.

To apply the PB calculations of gel water volumes to OPC-SCM, a constant, β , is introduced. The constant modifies the PB gel water volume predictions with the additional data provided by the pore partitioning models' thermodynamic calculations. The constant β is the amount of gel water predicted by the PB model for OPC (that is, 19% of gel solid volumes) reduced by the volume of released water by the major phases, all taken as a ratio of the total volume of C-S-H predicted by the thermodynamic calculations. This approach allows for more precise calculation of gel water volumes for OPC-SCM because it accounts for thermodynamically calculated volumes of C-S-H. This extension of PB for gel water volume calculation is important in OPC-SCM systems because C-S-H phases comprise a major portion of the hydrated phases and, consequently, contain a major part of the gel pores, that contain the gel water.

3. The calculation of the constant, β

Table 1—Chemical compositions of SCMs and OPC used in this study (mass %)³⁸⁻⁴⁸

	SiO ₂	Al ₂ O ₃	Fe ₂ O ₃	CaO	SO ₃	Na ₂ O _{eq}	MgO
FAF	51.60	22.64	8.89	7.55	0.73	1.06	1.64
FAC	39.04	19.79	5.67	21.43	1.65	3.52	4.63
Slag	35.23	10.72	0.86	38.65	1.52	0.31	10.75
	C ₃ S*	C ₂ S*	C ₃ A*	C ₄ AF*	SO ₃	Na ₂ O _{eq}	MgO
OPC	61.43	14.20	6.94	10.20	3.32	0.18	2.25

*Cement chemistry notation is used for cement phases (C is CaO, S is SiO₂, A is Al₂O₃, and F is Fe₂O₃).

$$\beta = \frac{V_{gw,PB} - V_{released}}{V_{C-S-H}} \quad (4c)$$

where $V_{gw,PB}$ is the volume of gel water calculated for OPC from PB using Eq. (1) (m³ [ft³]). Note that this calculation is performed for the base OPC system and the calculated β is then assumed to remain constant when a part of cement is replaced with SCM. The PB equation for gel water volume is used as a baseline to establish the relationship between gel water volume and the volume of reacted material in an OPC system. This information is used in conjunction with the volume of C-S-H calculated by Eq. (4b), and the water released from other hydrated phases calculated by Eq. (4a), as obtained from the thermodynamic modeling,¹¹ to compute a constant value, which is used in the final step of the gel water calculation.

4. The calculation of total gel water volume (m³ [ft³]) of the OPC-SCM system

$$V_{gw} = V_{released} + \beta V_{C-S-H} \quad (4d)$$

Capillary water calculations—The balance of the water in the system is assumed to be capillary water. The pore partitioning model calculates capillary water volume (m³ [ft³]) as follows

$$V_{cw} = V_w - (V_{gw} - V_{released}) \quad (5)$$

where V_{cw} is capillary water (m³ [ft³]); V_w (m³ [ft³]) is excess unreacted water from GEMS3K.

Unreacted material and chemical shrinkage calculations—The pore partitioning model computes the volumes of unhydrated and unreacted material as well as chemical shrinkage algebraically based on the thermodynamic results and normalizes these results by total initial system volume.

ANALYSIS

The pore partitioning model was used to simulate blended mixtures of OPC Type I with Class C fly ash (FAC), Class F fly ash (FAF), and slag at a w/b of 0.42. SCM and OPC chemical compositions were obtained as typical values from literature³⁸⁻⁴⁸ and are summarized in Table 1. Blaine fineness of the cements was assumed to be 375 m²/kg (1830.90 ft²/lb), and the water density was assumed to be 1000 kg/m³ (62.43 lb/ft³). All calculations were done at room temperature (that is, 23°C [73.4°F]).

Because SCM reactivity is a major factor in the evolution of hydrating paste phases, the pore partitioning model

was run for multiple DoR and SCM replacement levels to capture trends and separate effects of SCM replacement level, SCM reactivity, and SCM chemical composition on paste properties.

First, the pore partitioning model was compared to the classic PB model for plain OPC. Slag, Class C fly ash (FAC), and Class F fly ash (FAF) were then added to the model and presented in the familiar “Powers-Brownyard” format for reasonable reactivity (40%, 20%, and 20% for slag, Class C, and Class F fly ash, respectively) and replacement (40% by volume) levels,⁴⁹ to describe the influence of the chemical composition of the binder on phase and pore volumes of the hydrating pastes. To further clarify the influence of SCM composition on the density and gel pore structure of the cement, gel water/gel total ratios (that is, gel water/(gel solids + gel water)) were calculated and compared to the PB model’s constant value of 0.28.

The influence of SCM replacement volumes on important paste phases (gel solids, C-S-H, and C-S-H C/S) are shown to elucidate how variable SCM replacement levels influence the hydrating paste. The role of SCM reactivity on important paste properties such as pore size distribution, and the volumes of gel solids and unreacted materials were evaluated using the pore partitioning model.

RESULTS AND DISCUSSION

Model validation for OPC

Figure 1 illustrates the changes in the phase volumes as a function of the degree of hydration for OPC with w/b of 0.42. The results of the pore partitioning model (Fig. 1(b)) are compared with the PB model (Fig. 1(a)). It can be seen that the two models show good agreement for the OPC paste at all degrees of hydration. Phase volumes, porosity (gel and capillary), and chemical shrinkage values are nearly identical for the two models. The only major difference is that the pore partitioning model shows that hydration ceases at a DoH of 95%, whereas the PB-modeled system fully hydrates (that is, DoH of 100%). This discrepancy is minor and is likely a consequence of the fact that the PB model is based on systematic empirical investigations of the reactions of multiple cement types (based on cements from the 1940s) and water, whereas the pore partitioning model’s thermodynamic component incorporates the chemical composition of the OPC in the calculations. Additionally, the PB model assumes a constant value for chemical shrinkage (6.5 mL/100 gram [1.8 in.³/lb] of cement reacted), while the pore partitioning model shrinkage results are also a function of paste chemical composition. The chemical composition of the cement will influence the specific hydra-

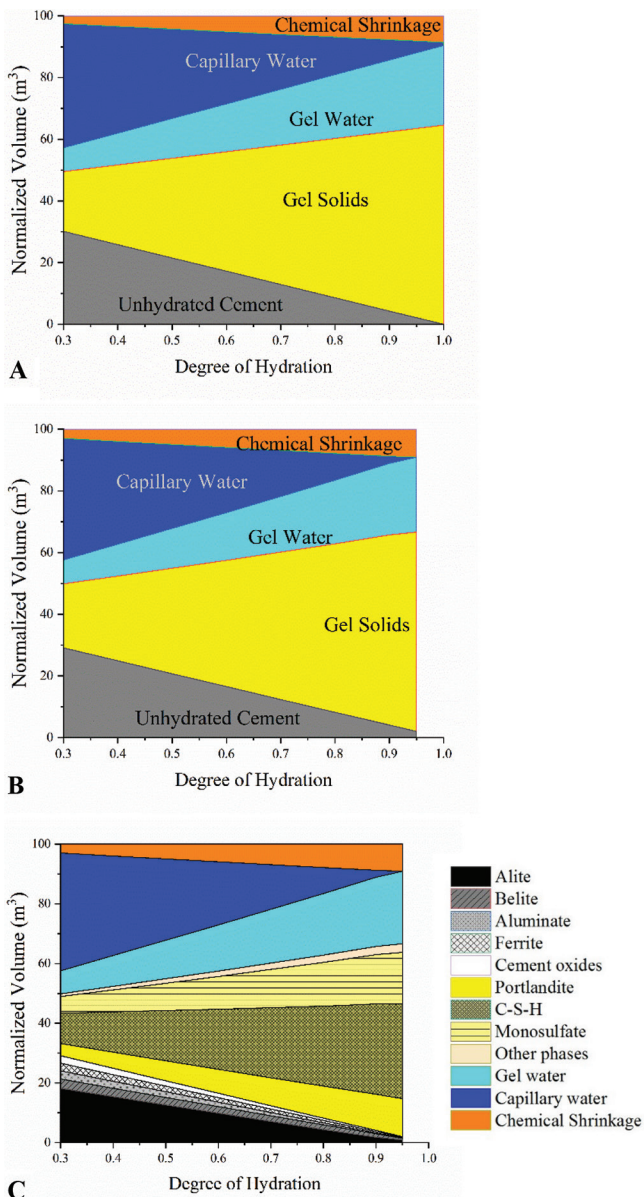


Fig. 1—Changes in phases as function of degree of hydration for OPC with w/b of 0.42: (a) Powers Model; (b) Pore Partitioning Model; and (c) Pore Partitioning Model (detailed phases).

tion products that are formed, as well as the pore structure of the hydrating pastes.^{50,51}

A major benefit of the thermodynamic approach used in the pore partitioning model is that detailed phase assemblages can be predicted for the unreacted and hydrating pastes. Figure 1(c) shows this breakdown for the plain OPC system as a function of the degree of hydration, as predicted by the pore partitioning model. Precise information on the volumes of phase assemblages has an important implication for modeling: the data provided by the thermodynamic calculations can be used to modify and refine the calculations of the PB model (such as those for gel water) based on the ability to compute the volumes of water bound to each phase (for example, C-S-H and other gel solids). The detailed phase assemblage information is also useful for practical purposes. For example, because C-S-H is funda-

mental to strength development and durability of a concrete, it is helpful to be able to quantify the volume of C-S-H in a hydrating paste. Similarly, the ability to predict the CH phase is critical in the assessment of a concrete mixture's resistance to steel corrosion⁵² or salt damage.⁵³ In addition, pH and pore solution conductivity data provided by the thermodynamic calculations are useful for prediction of durability-related properties of the hardened pastes.

Agreement between the pore partitioning model and PB has been established for the calculation of total gel volumes of OPC pastes, which is a critical factor in resistance to carbonation and chloride ingress.⁵⁴ While the PB model predicts a constant value of 0.28 for the gel water/gel total ratio, the pore partitioning model predicts a constant value of 0.27 in OPC (Fig. 2). This is due to slightly higher gel solid volumes predicted by the pore partitioning model (Fig. 1(b)). The discrepancy is minor and likely a result of the consideration of chemical composition in the pore partitioning model. Overall, it can be concluded that the pore partitioning model shows good agreement with the PB model for OPC.

The pore partitioning model was used to simulate phase and pore structure in pastes containing different SCMs, with different chemical compositions. OPC systems with replacement by slag, FAC, and FAF were simulated to evaluate and separate chemical effects from dilution effects. The chemical composition of the binder will influence the specific hydration products formed, as well as the pore structure of the pastes. The replacement of OPC by SCM results in a change in the binder chemical composition as compared to plain OPC.

The addition of slag, FAF, and FAC to the pore partitioning model shows exactly how phase and pore volumes change in the hydrating pastes when 40% (by volume) of the OPC is replaced by these SCMs as shown in Fig. 3. To simplify the comparisons, DoRs representative of previously reported literature values are used. The DoR of slag is modeled at 40%, FAC at 20%, and FAF at 20%.⁵⁵⁻⁵⁷ There are striking differences between the phase and pore volumes of OPC pastes versus OPC-SCM pastes as shown in Figures 2 and 3. The volumes of gel solid are considerably lower in all of the OPC-SCM systems as compared to OPC. This is due in part to the lower assumed reactivity of the SCMs, and the fact that as a consequence of this lower reactivity, the OPC-SCM systems all have roughly 20% of the total volume comprised of unreacted material at a DoH of 100%, whereas the OPC system is assumed to fully hydrate. Hence, gel solid volumes will be higher for OPC-SCM if the SCM fully reacts, as illustrated in Fig. 4. Similarly, the capillary water volumes in the OPC-SCM pastes are higher than OPC: again, due to the lower assumed reactivity of SCM relative to OPC. Despite these heterogeneities, chemical shrinkage volumes are only slightly lower in OPC-SCM pastes than plain OPC. These lower chemical shrinkage values in OPC-SCM systems relative to OPC are expected: SCMs react slower than OPC hydrates, which results in lower chemical shrinkage values. This is also why the OPC-slag chemical shrinkage values are higher than the OPC-fly ash values: slag reactivity is greater than FAC or FAF.

Although the model results for the pore volumes in plain OPC versus OPC-SCM pastes are noticeably different, the

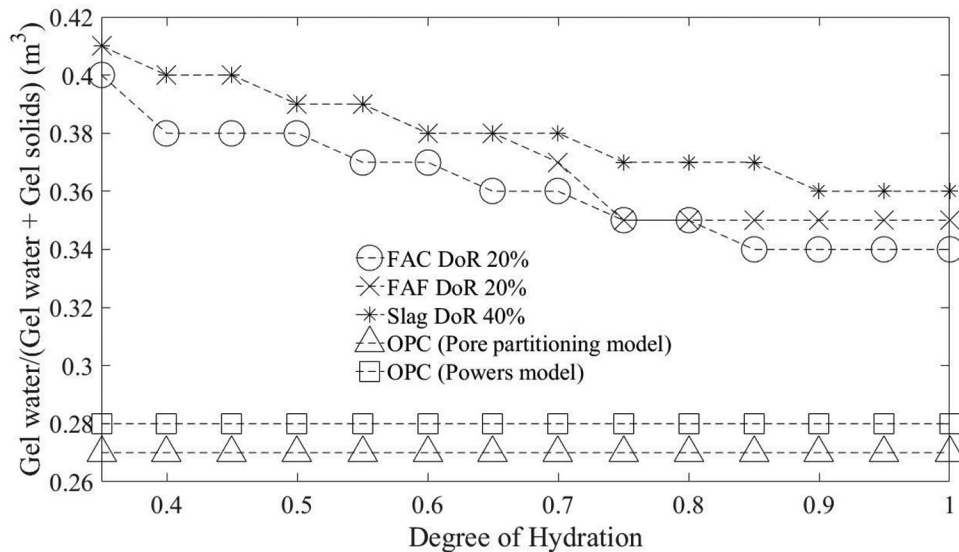


Fig. 2—Gel water/(gel water + gel solid) ratio for OPC and OPC-SCM systems. Simulations were done for w/b of 0.42 and at 40% (vol) SCM replacement.

differences in phase and pore volumes between the modeled OPC-SCM systems are not as striking, despite clear differences in the SCM chemical compositions. In other words, although the modeled SCM chemical compositions are different from one another, the model results for all of the OPC-SCM systems are more similar to each other than they are to OPC. Gel solid, gel porosity, and capillary porosity volumes are almost identical in the OPC-FAC and FAF systems. Similarly, these volumes are closer in value to OPC-slag than OPC-slag is to plain OPC. This suggests that chemical composition is not the only influence on the performance of a mixture. This is an important finding, because ASTM C618⁵⁸ considers SCM chemical composition one of the deciding factors in whether certain SCMs are considered to be “in-specification” and hence useable for replacing OPC for use in concrete production.

Reviewing the model outputs for OPC-FAF (Fig. 3(b)) and OPC-FAC (Fig. 3(c)), it is observed that chemical shrinkage, phase, and pore volumes are nearly identical. The OPC-slag (Fig. 3(a)) differs slightly from the OPC-fly ash pastes in that more of the binder reacts; hence, there are lower capillary water and higher gel volumes. Nevertheless, the OPC-slag paste is more similar to OPC-fly ash than to plain OPC in terms of the percent of gel solids, gel porosity and capillary porosity, as well as chemical shrinkage.

The differences between OPC and OPC-SCM pastes are also apparent in the gel water volume ratios ((gel water)/(gel water + gel solid)) of the pastes (Fig. 2). Whereas the gel water volume ratios in OPC systems are a constant value of 0.27, the OPC-SCM values range from 0.41 to 0.34 and tend to decrease as the systems hydrate. The decrease in this ratio is partly due to the fact that DoR is kept constant in the pore partitioning model as DoH increases. However, this may also indicate a change in the proportion of gel pores relative to overall gel as the OPC-SCM pastes hydrate. This interpretation is supported by the pore partitioning model results, which show a shift from short to long chained C-S-H variants as the pastes hydrate (Fig. 4, 5, and 6). In

general, however, the higher gel water volume ratios in the OPC-SCM pastes are reflective of the lower volumes of gel solids in these systems. This is expected because SCM reactivity is lower than cement degree of hydration.

Influence of SCM replacement level

The dilution of OPC by SCM can influence the hydration products formed in the paste.⁵⁹ The SCM itself is known to create nucleation sites for the growth of hydration products, notably C-S-H.⁵⁹⁻⁶¹

Figure 4 shows how total gel solid volumes for FAF and slag compare at replacement levels of 20, 40, 60, and 80% as a function of both DoH and DoR, and Fig. 5 and 6 show the particular C-S-H composition formed in these systems for the same replacement levels. As noted earlier, the calcium-to-silica (C/S) ratio of C-S-H changes as replacement levels increase, transitioning from the low-C/S C-S-H to high-C/S C-S-H variant as volumetric replacement levels increase. This may have important implications because the C-S-H structure impacts the final compressive strength of the hardened cement.⁶² A lower C/S ratio is associated with improved durability and strength gain in hydrated pastes: prior experimental work has shown that a low (≤ 1.5) C/S C-S-H characteristic of OPC-SCM mixtures binds alkali better than the higher C/S C-S-H typically found in OPC systems.⁶³ Higher alkali binding in pastes can reduce the potential for reactions with reactive aggregates. Similarly, compressive strength has also been shown to increase as the C/S of C-S-H in cement decreases below 1.5.⁶²

Looking at plots of gel solid volumes for 20% and 80% replacement levels for FAF (Fig. 4(a) and 4(g)) and slag (Fig. 4(b) and 4(h)), it is clear that gel solid volumes increase with DoR almost proportionally in the 20% replacement level cases. In contrast, the 80% replacement gel solid volumes appear to increase almost linearly with DoH. The 40% and 60% cases (Fig. 4(c), 4(d), 4(e), and 4(f)) fall somewhere between these end members. This is consistent with expectations. In the highly diluted 80% system, Calcium Hydroxide

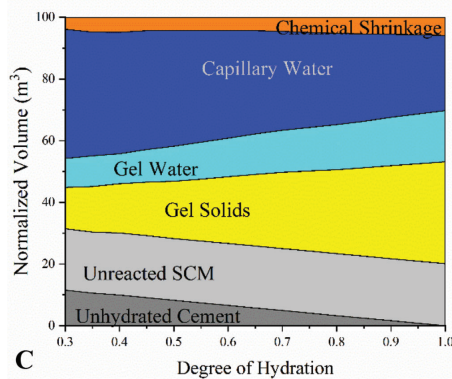
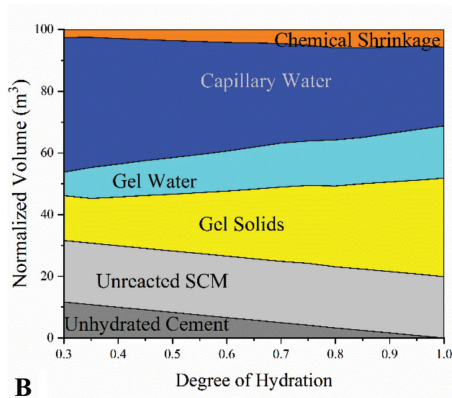
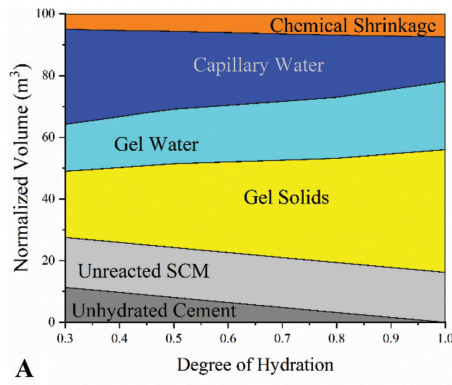


Fig. 3—Normalized volume of phases OPC + 40% SCM systems: (a) OPC-Slag with slag DoR of 40%; (b) OPC-FAC with FAC DoR of 20%; and (c) OPC-FAC with FAF DoR of 20%.

(CH) production is not sufficient to react with all SCM until higher DOHs. In the 20% system, there is a large proportion of OPC and hence ample calcium hydroxide (CH) for the pozzolanic reaction to proceed. Again, trends between OPC-FAC and OPC-slag are strikingly similar, despite dissimilar chemical compositions, and despite the hydraulic character of the slag. Although it might be expected that OPC-slag would result in gel solid volumes similar to plain OPC (given the hydraulic character of both), the pore partitioning model results indicate that the volumetric replacement of OPC by SCM (regardless of SCM composition) is a driving factor in the evolution of hydrating paste properties.

In addition to replacement volumes of SCM, the reactivity of the SCM also influences paste properties. For example, Fig. 4 illustrates that SCM DoR heavily influences gel solid

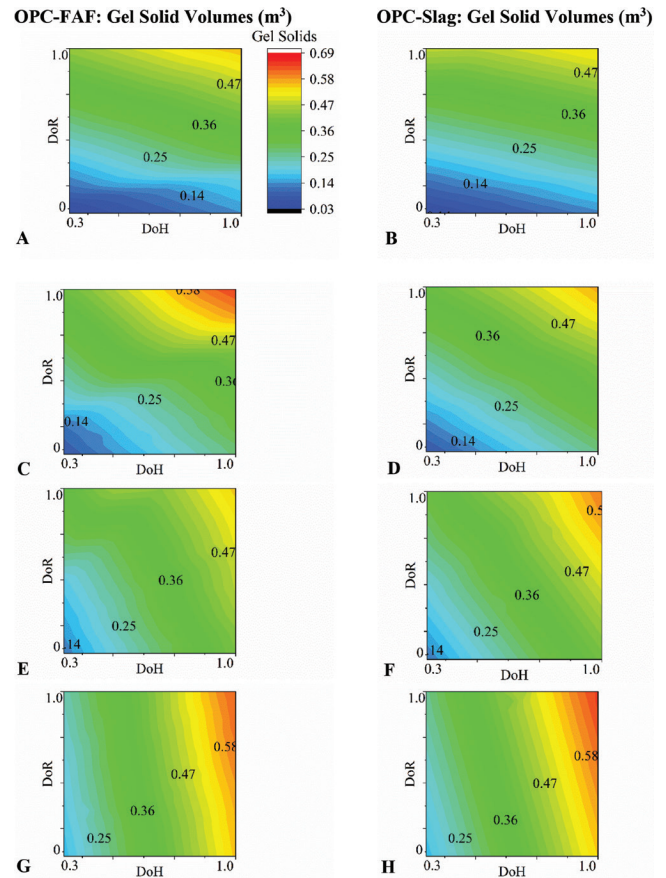


Fig. 4—Gel solid and C-S-H volumes for pastes of varying replacement levels A and B = 20% replacement; C and D = 40% replacement; E and F = 60% replacement; G and H = 80% replacement.

volumes: the role of SCM DoR is discussed in greater detail in Section 5.3. In all cases, CH availability at higher SCM replacement level is the limiting factor in the formation of gel solids, and the pore partitioning model demonstrates how the formation and pozzolanic consumption of CH changes with SCM reactivity and replacement volumes.

An additional benefit of the pore partitioning model is the ability to predict detailed phase assemblages of hydrating pastes, including the variants of C-S-H. GEMS3K models two major variants of C-S-H: Jennite and tobermorite, each with two subtypes (D and H). Jennite typically has a higher C/S⁶⁴ and a typically longer chain length than tobermorite.⁵⁴ The C/S and morphology of the C-S-H influence cement strength and cement density, and hence are important properties to quantify in OPC-SCM systems. Previous work⁶⁵ has established a transition from high-to-low C/S C-S-H as OPC-SCM pastes hydrate. Generally, this is related to the pozzolanicity of the SCM and attendant effects on pore solution alkalinity. Typically, the greater the pozzolanic reaction, the lower the C/S ratio of the cement.⁶⁵ A C/S ratio of <1.5 has been demonstrated to be optimal for the development of compressive strength of the hardened pastes: experimental evidence shows that compressive strengths of C-S-H pastes increases with decreasing C/S.^{62,66}

A reduction in the paste C/S ratio of C-S-H ratio from fly ash replacement is a consequence of a reduction in pore solution alkalinity from the pozzolanic reaction itself.⁶³ The

OPC-FAF: C-S-H Jennite Volumes (m³) **OPC-Slag: C-S-H Jennite Volumes (m³)**

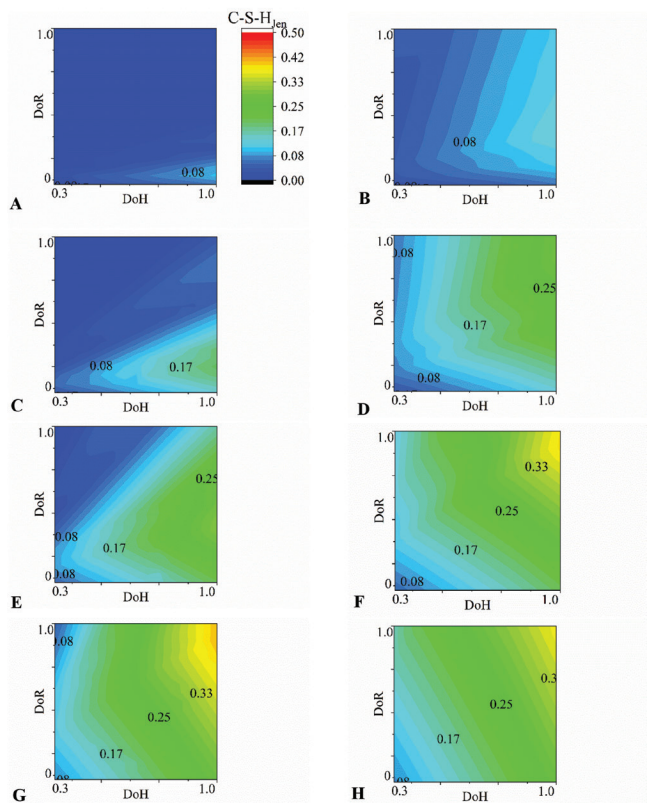


Fig. 5—C-S-H (Jennite) volumes for OPC-FAF and OPC-Slag systems at varying replacement levels: A and B = 20% replacement; C and D = 40% replacement; E and F = 60% replacement; G and H = 80% replacement.

pozzolanic reaction releases more alkalis, which become bound to C-S-H with a lower C/S.⁶⁷ The initial amounts of CaO and SiO₂ in the binder impact the amount of calcium and silica in the paste (and pore solution). When more silica is available, the C/S ratio of the hydrates is lower. The resulting removal of alkalis from the pore solution lowers the overall solution alkali content. In contrast, higher calcium levels increase the C/S ratio of the hydrates, which reduces the amount of alkalis removed from the solution and creates a high-alkali pore solution.

Figures 6(a), 6(c), 6(e), and 6(g) illustrate the effect of pozzolanicity on C-S-H C/S. Examining these figures on the y-axis, moving from bottom to top (which represents increasing DoR/pozzolanicity), it is apparent that at all fly ash replacement levels, the volume of C-S-H tobermorite (low C/S) increases. This indicates that as expected, the more reactive the fly ash, the greater the C/S ratio of the pastes. This effect is not as strongly observed in the OPC-slag system (Fig. 5(b), 5(d), 5(f), and 5(h)), which is likely a consequence of the hydraulic character of the slag.

It is noteworthy that the C-S-H tobermorite (low C/S) variant tends only to form at intermediate-to-high SCM DoR and DoH, particularly in the fly ash systems. In contrast, C-S-H jennite (Fig. 5) is most responsive to changes in cement DoH. These results suggest that C-S-H jennite may be less impacted by the SCM addition than C-S-H tobermorite. These results may also help explain why the gel water ratio shown in Fig. 3 decreases as pastes hydrate.

OPC-FAF: C-S-H Tob Volumes (m³) **OPC-Slag: C-S-H Tob Volumes (m³)**

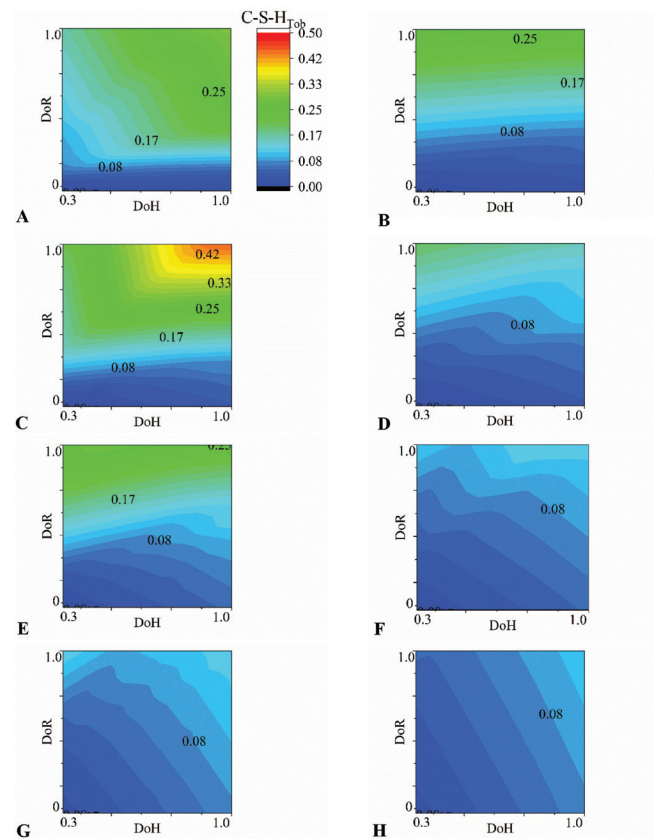


Fig. 6—C-S-H (Tobermorite) volumes for OPC-FAF and OPC-Slag systems at varying replacement levels A and B = 20% replacement; C and D = 40% replacement; E and F = 60% replacement; G and H = 80% replacement.

Influence of SCM DoR

Figures 7(a) and 7(b) show how SCM reactivity influences the relative proportions of hydrated paste phase and pore volumes that form at a 40% SCM replacement level. Figure 7(a) shows the proportions of unreacted material, gel solids, and total porosity normalized to the total material volume for each system. Total porosity is the sum of capillary and gel porosities, and chemical shrinkage. Transposed on top of the pore partitioning model results in Fig. 7(a) are three lines, representing data fitted from nine data points. The first two data points, shown in the plot as the uppermost points on the bottom (x) and right (z) axes, are the results predicted by PB for a plain OPC system with a w/b of 0.30 at DoH = 0 and DoH = 100%. DoH = 50% is plotted near the middle of the line. The second set of points, found below the 0.30 w/b case are PB's predictions for a w/b of 0.42 at DoH = 0, DoH = 50%, and DoH = 100%; and the third set are the predictions for a w/b of 0.54 at DoH = 0, DoH = 50%, and DoH = 100%. The purpose of these lines is to provide a benchmark for the expected phase and pore volumes in an equivalent OPC system. The specific w/b were chosen to illustrate how OPC-SCM pastes of a constant 0.42 w/b compare with plain OPC pastes of reasonably higher and lower w/b. The reason for this comparison is that an OPC-SCM paste must have comparable phase and pore volumes to a plain OPC system for the mixture to be truly

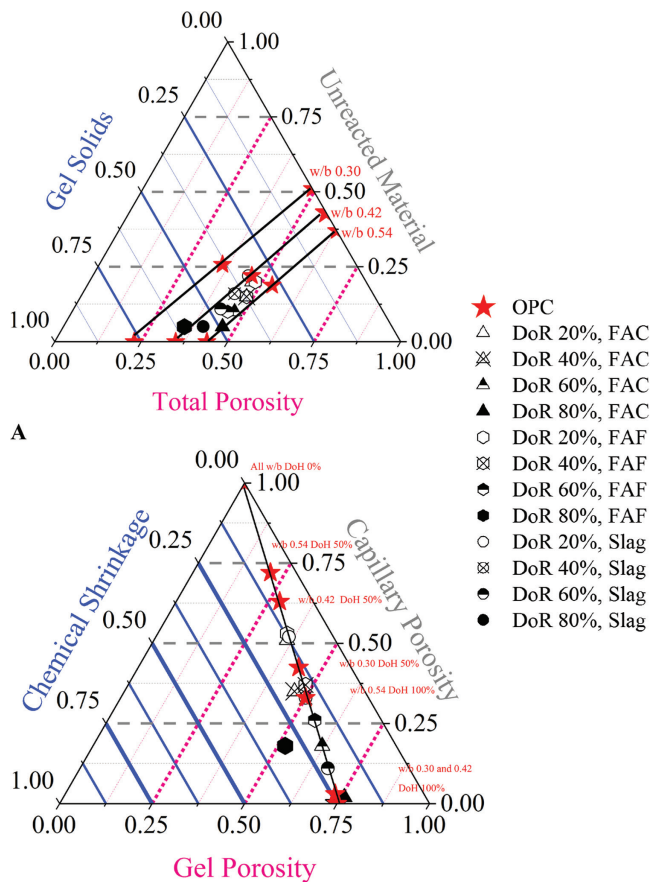


Fig. 7—(a) relative normalized proportions of unreacted material, total porosity, and gel solids for multiple hydrated OPC-SCM systems of various SCM reactivities modeled by pore partitioning model. All SCM replacement levels are 40% by volume, and all cement in OPC-SCM is fully hydrated; and (b) relative normalized proportions of gel porosity, capillary porosity, and chemical shrinkage for multiple hydrated OPC-SCM systems of various reactivities as modeled by pore partitioning model. All SCM replacement levels are 40% by volume, and all cement in OPC-SCM is fully hydrated. Black lines transposed on figure show PB model results for plain OPC systems of w/b of 0.30, 0.42. Stars present 0.54 at 0%, 50%, and 100% DoH.

equivalent. The lines also allow for rapid determination of how the addition of SCMs of various compositions (at a w/b of 0.42) and reactivities compare to plain OPC mixtures.

The first observation to make from Fig. 7(a) is that although the SCM containing pastes are designed at a w/b of 0.42, the FAF and FAC containing pastes tend to plot between the lines for OPC w/b 0.42 and 0.54 at modeled SCM reactivity levels of 40% and 60%. The FAC paste modeled at 80% DoR plots exactly on the 0.54 line. In other words, these SCM containing mixtures are more equivalent to a plain OPC system designed with a w/b of 0.54 than to their w/b of 0.42, in terms of total porosity and gel solid volumes. Considering that these pastes have higher volumes of both unreacted material and water (as less is consumed by the reactions) than plain OPC, this result makes sense. In contrast, the slag systems tend to plot closer to the 0.42

line: this is likely a result of the hydraulic nature of slag, which may result in a system more similar to OPC than one designed with a pozzolan.

A second observation to make from Fig. 7(a) is that the relative volumetric proportions of the gel solids, unreacted material, and total porosity for each modeled OPC-SCM system have more in common with the other OPC-SCM systems (that is, various SCMs) of the same modeled reactivity than with the systems containing the same SCM but different reactivities. SCM reactivity is represented on the plot by a shape fill gradient (with the highest reactivity SCMs having a solid fill, and lowest reactivities having an empty fill, and so on). SCM type is represented on the plots by shape geometry (that is, FAC is a triangle, slag is a circle). There is a clear clustering of data points based on reactivity, but not based on SCM type. This is indicative of the critical role SCM reactivity plays in driving the evolution of paste properties. If chemical composition were the primary factor driving the hydrated paste phase and pore assemblages, then the data points would cluster more based on SCM type than reactivity. This is an important observation because SCM chemical composition is a primary consideration under ASTM C618 in determining whether a pozzolan is considered to be “in specification” and useable as a replacement for OPC. These results suggest that paste properties may be driven more by the reactivity of SCM than by chemical composition and suggest that performance-based approaches for SCM specifications ought to be evaluated. Although ASTM C618⁵⁸ does also have a physical performance-based element in that a certain strength activity index (SAI) must be achieved, the SAI can be significantly affected by the cement used in the test and the chemical composition restrictions imposed by ASTM C618⁵⁸ still disqualify a considerable fraction of SCM, which could otherwise potentially be useable as a partial replacement for OPC. As such, reactivity tests may be more important than a Class C or Class F determination for evaluating SCM for use in cements.¹⁶

Another observation to make from Fig. 7(a) is that for the FAF-, FAC-, and slag-containing systems, as the reactivity of the SCM increases, the proportion of unreacted material decreases, and the volume of gel solid increases, and this increase can be substantial. Total pore volume proportions also tend to decrease with increasing DoR, but the differences are small. However, it is noteworthy that although total pore volumes of the pastes do not substantially differ based on DoR, the pores do tend to become refined at higher modeled SCM reactivities (that is, there is a higher volume of gel pores to total pores) (Fig. 7(b)).

Figure 7(b) shows the relative distribution of pore sizes (capillary, gel, and chemical shrinkage) for the same OPC-SCM pastes, as well as a plain OPC paste designed at w/b of 0.42. With the exception of FAF modeled at an 80% DoR, all of the OPC-SCM pastes transition from capillary pore dominated systems at DoR of 20% and 40%, to gel pore dominated systems at modeled DoRs of 60% and 80%. FAC with a DoR modeled at 80% is nearly identical to plain OPC in terms of the pore size distribution. This transition from capillary to gel pore dominated systems with increasing DoR is indicative of the fact that more material is reacting

at higher DoR (Fig. 7(a)) and is exactly the result that would be expected.

Finally, as shown in Fig. 7(b), at DoRs modeled at 20% and 40%, the relative pore size distributions are nearly identical for OPC-FAC, OPC-FAF, and OPC-slag. Some heterogeneities are observed between SCMs as DoR increases to 60% and 80%. Nevertheless, the SCM reactivity (as opposed to the SCM composition) again appears to be the primary control on pore size distributions. If chemical composition were the driving factor, then the data points would be expected to cluster based on SCM type rather than SCM reactivity. Here, it is apparent that until unrealistically high, (that is, 60+%) modeled reactivities, the OPC-SCM pastes are clustering based on the SCM reactivity and not SCM type.

CONCLUSIONS

Thermodynamic calculations were used to extend the Powers-Brownyard model to estimate phase and pore volumes in hydrating OPC-SCM pastes. The model compared well to the classic PB model for OPC phase volume predictions. The influence of SCM chemistry, replacement level, and reactivity were evaluated.

The pore partitioning model allows for direct comparison between the evolution of paste phase and pore volumes in hydrating OPC and OPC-SCM systems. This addresses a major need in cement science insofar as the development of OPC-equivalent OPC-SCM pastes relies on a detailed understanding of how hydration products and different types of porosity develop when different binders, replacement levels, and w/b are used. Because the pore partitioning model can separate and clarify effects of OPC and SCM reaction rates and OPC and SCM compositions, it was possible to simulate the effects of varying these properties for a large number of modeled pastes.

The model results show that the SCM reactivity is a driving influence on the pastes. While all of the modeled OPC-SCM systems developed different phase and pore volumes compared to OPC, the differences between SCM types are less pronounced when considering only differences in chemical composition of the SCM. However, SCM reactivity is a key factor in the formation of the observed phase and pore volumes in hydrated OPC-SCM pastes and should be considered a critical parameter in a performance-based specification for use of SCM in cementitious systems. When OPC-SCM systems with a w/b of 0.42 are compared to plain OPC, the pore partitioning model shows that most of the OPC-SCM hydrated paste properties have phase and pore volume proportions that are more similar to OPC with a higher w/b . Furthermore, the pore partitioning model demonstrates that the reactivity and replacement level of the SCM has a considerable influence on the type and morphology of the gel solids that are formed. The more reactive the SCM, the lower the C/S ratio of the C-S-H. This is of fundamental importance to the development of durability-related properties of cements.

The model presented in this work is of substantial impact in furthering the understanding of the reactions between OPC and different SCMs. The model fills a critical knowl-

edge gap by incorporating thermodynamic principles with established cement kinetics and empirical knowledge embodied in the work and modeling of Powers-Brownyard to provide detailed predictions on pore and phase volumes, which can be used to design pastes optimized for durability performance, and to elucidate structure/property relationships of hardened concrete.

AUTHOR BIOS

ACI member Deborah Glosser is a PhD Student and ARCS Scholar at Oregon State University, Corvallis, OR. She received her MS in geophysics from the University of Pittsburgh, Pittsburgh, PA. Her research interests include thermodynamic and multi-physics modeling of cement and metals-based materials.

ACI member Vahid Jafari Azad is a Structural Engineer at WSP USA and a Researcher on computational infrastructure material science and multi-scale/multi-physics modeling for durability of concrete structures. He received his BS, MS, and PhD from the University of Tehran, Tehran, Iran.

ACI member Prannoy Suraneni is an Assistant Professor in the Department of Civil, Architectural, and Environmental Engineering at the University of Miami, Miami, FL. He received his BTech from Indian Institute of Technology Madras, Chennai, India; his MS from the University of Illinois at Urbana-Champaign, Champaign, IL; and his PhD from ETH Zurich, Zurich, Switzerland. His research interests include alternate and supplementary cementitious materials, chemical admixtures, and concrete durability.

ACI member O. Burkan Isgor is the John and Jean Loosley Faculty Fellow in the School of Civil and Construction Engineering at Oregon State University. He is Chair of the ACI Committee 222, Corrosion of Metals in Concrete, and is a member of ACI Committees 236, Material Science of Concrete, and 365, Service Life Prediction. His research interests include corrosion of steel in concrete, service-life modeling, and nondestructive testing.

W. Jason Weiss, FACI, is the Edwards Distinguished Professor of Engineering and Head of the School of Civil and Construction Engineering at Oregon State University. He is Chair of ACI Committee 231, Properties of Concrete at Early Ages, and is a member of ACI Subcommittee 318-A, General, Concrete, and Construction (Structural Concrete Building Code). His research interests include fluid transport in concrete as well as service-life modeling.

ACKNOWLEDGMENTS

The authors acknowledge financial support for this research provided by: The National Science Foundation (CMMI: 1728358) and Federal Highway Administration (DTFH61-06-H-00011 [Work Plan 25]) Pooled Fund Study TPF-5(205).

REFERENCES

1. Suraneni, P., and Weiss, J., "Examining the Pozzolanicity of Supplementary Cementitious Materials Using Isothermal Calorimetry and Thermogravimetric Analysis," *Cement and Concrete Composites*, V. 83, 2017, pp. 273-278. doi: 10.1016/j.cemconcomp.2017.07.009
2. Jafari Azad, V., and Isgor, O. B., "Modeling Chloride Ingress in Concrete with Thermodynamically Calculated Chemical Binding," *International Journal of Advances in Engineering Sciences and Applied Mathematics*, V. 9, No. 2, 2017, pp. 97-108. doi: 10.1007/s12572-017-0189-2
3. Powers, T., and Brownyard, T., "Studies of the Physical Properties of Hardened Portland Cement Paste," *Bulletin*, V. 22, 1946.
4. Jensen, O. M.; Hansen, P. F.; Coats, A. M.; and Glasser, F. P., "Chloride Ingress in Cement Paste and Mortar," *Cement and Concrete Research*, V. 29, No. 9, 1999, pp. 1497-1504. doi: 10.1016/S0008-8846(99)00131-3
5. Jensen, O. M., and Hansen, P. F., "Water-Entrained Cement-Based Materials: I. Principles and Theoretical Background," *Cement and Concrete Research*, V. 31, No. 4, 2001, pp. 647-654. doi: 10.1016/S0008-8846(01)00463-X
6. Igarashi, S.-i.; Kawamura, M.; and Watanabe, A., "Analysis of Cement Pastes and Mortars by a Combination of Backscatter-Based SEM Image Analysis and Calculations Based on the Powers Model," *Cement and Concrete Composites*, V. 26, No. 8, 2004, pp. 977-985. doi: 10.1016/j.cemconcomp.2004.02.031
7. Habel, K.; Viviani, M.; Denarié, E.; and Brühwiler, E., "Development of the Mechanical Properties of an Ultra-High Performance Fiber Rein-

- forced Concrete (UHPC),” *Cement and Concrete Research*, V. 36, No. 7, 2006, pp. 1362-1370. doi: 10.1016/j.cemconres.2006.03.009
8. Lam, L.; Wong, C. S.; and Poon, C. S., “Degree of Hydration and Gel/Space Ratio of High-Volume Fly Ash/Cement Systems,” *Cement and Concrete Research*, V. 30, No. 5, 2000, pp. 747-756. doi: 10.1016/S0008-8846(00)00213-1
9. Brouwers, H. J. H., “The Work of Powers and Brownard Revisited: Part 1,” *Cement and Concrete Research*, V. 34, No. 9, 2004, pp. 1697-1716. doi: 10.1016/j.cemconres.2004.05.031
10. Zeng, Q.; Fen-Chong, T.; Dangla, P.; and Li, K., “A Study of Freezing Behavior of Cementitious Materials by Poromechanical Approach,” *International Journal of Solids and Structures*, V. 48, No. 22-23, 2011, pp. 3267-3273. doi: 10.1016/j.ijsolstr.2011.07.018
11. Jafari Azad, V.; Suraneni, P.; Isgor, O. B.; and Weiss, W. J., “Interpreting the Pore Structure of Hydrating Cement Phases through a Synergistic Use of the Powers-Brownard Model, Hydration Kinetics, and Thermodynamic Calculations,” *Advances in Civil Engineering Materials*, V. 6, No. 1, 2017, p. 20160038 doi: 10.1520/ACEM20160038
12. Brouwers, H. J. H., “Paste Models for Hydrating Calcium Sulfates, Using the Approach by Powers and Brownard,” *Construction and Building Materials*, V. 36, 2012, pp. 1044-1047. doi: 10.1016/j.conbuildmat.2012.06.019
13. Feliu, S.; Gonzalez, J. A.; and Andrade, C., “Effect of Current Distribution on Corrosion Rate Measurements in Reinforced-Concrete,” *Corrosion*, V. 51, No. 1, 1995, pp. 79-86. doi: 10.5006/1.3293581
14. Igarashi, S.; Kawamura, M.; and Watanabe, A., “Analysis of Cement Pastes and Mortars by a Combination of Backscatter-Based SEM Image Analysis and Calculations Based on the Powers Model,” *Cement and Concrete Composites*, V. 26, No. 8, 2004, pp. 977-985. doi: 10.1016/j.cemconcomp.2004.02.031
15. Lothenbach, B.; Scrivener, K.; and Hooton, R. D., “Supplementary Cementitious Materials,” *Cement and Concrete Research*, V. 41, No. 12, 2011, pp. 1244-1256. doi: 10.1016/j.cemconres.2010.12.001
16. Snellings, R., “Assessing, Understanding and Unlocking Supplementary Cementitious Materials,” *RILEM Technical Letters*, V. 1, 2016, pp. 50-55. doi: 10.21809/rilemtechlett.2016.12
17. Durdziński, P. T.; Haha, M. B.; Zajac, M.; and Scrivener, K., “Phase Assemblage of Composite Cements,” *Cement and Concrete Composites*, V. 99, 2017, pp. 172-182. doi: 10.1016/j.cemconres.2017.05.009
18. Brouwers, H. J. H., “The Work of Powers and Brownard Revisited: Part 2,” *Cement and Concrete Research*, V. 35, No. 10, 2005, pp. 1922-1936. doi: 10.1016/j.cemconres.2005.04.009
19. Nadelman, E. I., and Kurtis, K. E., “Application of Powers’ Model to Modern Portland and Portland Limestone Cement Pastes,” *Journal of the American Ceramic Society*, V. 100, No. 9, 2017, pp. 4219-4231. doi: 10.1111/jace.14913
20. Parrot, L., and Killoh, D., “Prediction of Cement Hydration,” *British Ceramics Proceedings*, V. 35, 1984, pp. 41-53.
21. Lothenbach, B., and Winnefeld, F., “Thermodynamic Modelling of the Hydration of Portland Cement,” *Cement and Concrete Research*, V. 36, No. 2, 2006, pp. 209-226. doi: 10.1016/j.cemconres.2005.03.001
22. Lothenbach, B.; Matschei, T.; Moschner, G.; and Glasser, F. P., “Thermodynamic Modelling of the Effect of Temperature on the Hydration and Porosity of Portland Cement,” *Cement and Concrete Research*, V. 38, No. 1, 2008, pp. 1-18. doi: 10.1016/j.cemconres.2007.08.017
23. Kulik, D. A.; Wagner, T.; Dmytrieva, S. V.; Kosakowski, G.; Hingerl, F. F.; Chudnenko, K. V.; and Berner, U. R., “GEM-Selektor Geochemical Modeling Package: Revised Algorithm and GEMS3K Numerical Kernel for Coupled Simulation Codes,” *Computational Geosciences*, 2012, doi: 10.1007/s10596-012-9310-6
24. Dilnesa, B.; Lothenbach, B.; Le Saout, G.; Renaudin, G.; Mesbah, A.; Filinchuk, Y.; Wichser, A.; and Wieland, E., “Iron in Carbonate Containing AFm Phases,” *Cement and Concrete Research*, V. 41, No. 3, 2011, pp. 311-323. doi: 10.1016/j.cemconres.2010.11.017
25. Dilnesa, B. Z.; Lothenbach, B.; Renaudin, G.; Wichser, A.; and Kulik, D., “Synthesis and Characterization of Hydrogarnet $\text{Ca}_3(\text{Al}_x\text{Fe}_{1-x})_2(\text{SiO}_4)_y(\text{OH})_{4(3-y)}$,” *Cement and Concrete Research*, V. 59, 2014, pp. 96-111. doi: 10.1016/j.cemconres.2014.02.001
26. Dilnesa, B. Z.; Lothenbach, B.; Renaudin, G.; Wichser, A.; and Wieland, E., “Stability of Monosulfate in the Presence of Iron,” *Journal of the American Ceramic Society*, V. 95, No. 10, 2012, pp. 3305-3316. doi: 10.1111/j.1551-2916.2012.05335.x
27. Kulik, D. A., “Improving the Structural Consistency of C-S-H Solid Solution Thermodynamic Models,” *Cement and Concrete Research*, V. 41, No. 5, 2011, pp. 477-495. doi: 10.1016/j.cemconres.2011.01.012
28. Kulik, D. A., and Kersten, M., “Aqueous Solubility Diagrams for Cementitious Waste Stabilization Systems: II, End-Member Stoichiometries of Ideal Calcium Silicate Hydrate Solid Solutions,” *Journal of the American Ceramic Society*, V. 84, No. 12, 2001, pp. 3017-3026. doi: 10.1111/j.1551-2916.2001.tb01130.x
29. Kulik, D. A., and Kersten, M., “Aqueous Solubility Diagrams for Cementitious Waste Stabilization Systems. 4. A Carbonation Model for Zn-Doped Calcium Silicate Hydrate by Gibbs Energy Minimization,” *Environmental Science & Technology*, V. 36, No. 13, 2002, pp. 2926-2931. doi: 10.1021/es010250v
30. Lothenbach, B.; Pelletier-Chaignat, L.; and Winnefeld, F., “Stability in the System $\text{CaO-Al}_2\text{O}_3\text{-H}_2\text{O}$,” *Cement and Concrete Research*, V. 42, No. 12, 2012, pp. 1621-1634. doi: 10.1016/j.cemconres.2012.09.002
31. Matschei, T.; Lothenbach, B.; and Glasser, F. P., “Thermodynamic Properties of Portland Cement Hydrates in the System $\text{CaO-Al}_2\text{O}_3\text{-SiO}_2\text{-CaSO}_4\text{-CaCO}_3\text{-H}_2\text{O}$,” *Cement and Concrete Research*, V. 37, No. 10, 2007, pp. 1379-1410. doi: 10.1016/j.cemconres.2007.06.002
32. Moschner, G.; Lothenbach, B.; Rose, J.; Ulrich, A.; Figi, R.; and Kretzschmar, R., “Solubility of Fe-ettringite ($\text{Ca}_6[\text{Fe}(\text{OH})_6]_2(\text{SO}_4)_3\cdot 26\text{H}_2\text{O}$),” *Geochimica et Cosmochimica Acta*, V. 72, No. 1, Jan. 2008, pp. 1-18.
33. Moschner, G.; Lothenbach, B.; Winnefeld, F.; Ulrich, A.; Figi, R.; and Kretzschmar, R., “Solid Solution between Al-ettringite and Fe-ettringite ($\text{Ca}_6[\text{Al}_{1-x}\text{Fe}_x(\text{OH})_6]_2(\text{SO}_4)_3\cdot 26\text{H}_2\text{O}$),” *Cement and Concrete Research*, V. 39, No. 6, 2009, pp. 482-489. doi: 10.1016/j.cemconres.2009.03.001
34. Schmidt, T.; Lothenbach, B.; Romer, M.; Scrivener, K.; Rentsch, D.; and Figi, R., “A Thermodynamic and Experimental Study of the Conditions of Thaumassite Formation,” *Cement and Concrete Research*, V. 38, No. 3, 2008, pp. 337-349. doi: 10.1016/j.cemconres.2007.11.003
35. Lothenbach, B.; Matschei, T.; Moschner, G.; and Glasser, F. P., “Thermodynamic Modelling of the Effect of Temperature on the Hydration and Porosity of Portland Cement,” *Cement and Concrete Research*, V. 38, No. 1, 2008, pp. 1-18. doi: 10.1016/j.cemconres.2007.08.017
36. Snellings, R., “Solution-Controlled Dissolution of Supplementary Cementitious Material Glasses at pH 13: The Effect of Solution Composition on Glass Dissolution Rates,” *Journal of the American Ceramic Society*, V. 96, No. 8, 2013, pp. 2467-2475. doi: 10.1111/jace.12480
37. Durdziński, P. T.; Snellings, R.; Dunant, C.; Haha, M. B.; and Scrivener, K., “Fly Ash as an Assemblage of Model Ca-Mg-Na-Aluminosilicate Glasses,” *Cement and Concrete Research*, V. 78, 2015, pp. 263-272. doi: 10.1016/j.cemconres.2015.08.005
38. Tennis, P. D., *Chemical and Physical Characteristics of US Hydraulic Cements*, Portland Cement Association, Skokie, IL, 2016, pp.
39. Shehata, M. H., and Thomas, M. D. A., “The Effect of Fly Ash Composition on the Expansion of Concrete due to Alkali-Silica Reaction,” *Cement and Concrete Research*, V. 30, No. 7, 2000, pp. 1063-1072. doi: 10.1016/S0008-8846(00)00283-0
40. Aboustait, M.; Kim, T.; Ley, M. T.; and Davis, J. M., “Physical and Chemical Characteristics of Fly Ash Using Automated Scanning Electron Microscopy,” *Construction and Building Materials*, V. 106, Mar. 2016, pp. 1-10.
41. Hogan, F., and Meusel, J., “Evaluation for Durability and Strength Development of a Ground Granulated Blast Furnace Slag,” *Cement, Concrete and Aggregates*, V. 3, No. 1, 1981, pp. 40-52.
42. Lane, D. S., and Ozyildirim, H. C., “Evaluation of the Effect of Portland Cement Alkali Content, Fly Ash, Ground Slag, and Silica Fume on Alkali-Silica Reactivity,” *Cement, Concrete and Aggregates*, V. 21, No. 2, 1999, pp. 126-140. doi: 10.1520/CCA10426J
43. Lumley, J. S.; Gollop, R. S.; Moir, G. K.; and Taylor, H. F. W., “Degrees of Reaction of the Slag in Some Blends with Portland Cements,” *Cement and Concrete Research*, V. 26, No. 1, 1996, pp. 139-151. doi: 10.1016/0008-8846(95)00190-5
44. Thomas, M. D. A.; Scott, A.; Bremner, T.; Bilodeau, A.; and Donna, D., “Performance of Slag Concrete in Marine Environment,” *ACI Materials Journal*, V. 105, No. 6, Nov.-Dec. 2008, pp. 628-634.
45. Bleszynski, R.; Hooton, R. D.; Thomas, M. D. A.; and Rogers, C. A., “Durability of Ternary Blend Concrete with Silica Fume and Blast-Furnace Slag: Laboratory and Outdoor Exposure Site Studies,” *ACI Materials Journal*, V. 99, No. 5, Sept.-Oct. 2002, pp. 499-508.
46. Roy, D. M., and Idorn, G. M., “Hydration, Structure, and Properties of Blast Furnace Slag Cements, Mortars, and Concrete,” *ACI Journal Proceedings*, V. 79, No. 6, June 1982, pp. 444-457.
47. Laldji, S.; Phithaksouhthone, A.; and Tagnit-Hamou, A., “Synergistic Effect between Glass Frit and Blast-Furnace Slag,” *ACI Materials Journal*, V. 107, No. 1, Jan.-Feb. 2010, pp. 75-79.
48. Thomas, M. D. A., and Innis, F. A., “Effect of Slag on Expansion Due to Alkali Aggregate Reaction in Concrete,” *ACI Materials Journal*, V. 95, No. 6, Nov.-Dec. 1998, pp. 716-724.
49. Zeng, Q.; Li, K.; Fen-Chong, T.; and Dangla, P., “Determination of Cement Hydration and Pozzolanic Reaction Extents for Fly-Ash Cement Pastes,” *Construction and Building Materials*, V. 27, No. 1, 2012, pp. 560-569. doi: 10.1016/j.conbuildmat.2011.07.007

50. Lee, N. K.; Jang, J. G.; and Lee, H. K., "Shrinkage Characteristics of Alkali-Activated Fly Ash/Slag Paste and Mortar at Early Ages," *Cement and Concrete Composites*, V. 53, 2014, pp. 239-248. doi: 10.1016/j.cemconcomp.2014.07.007
51. De Weerd, K.; Haha, M. B.; Le Saout, G.; Kjellsen, K. O.; Justnes, H.; and Lothenbach, B., "Hydration Mechanisms of Ternary Portland Cements Containing Limestone Powder and Fly Ash," *Cement and Concrete Research*, V. 41, No. 3, 2011, pp. 279-291. doi: 10.1016/j.cemconres.2010.11.014
52. Jafari Azad, V., and Isgor, O. B., "A Thermodynamic Perspective on Admixed Chloride Limits of Concrete Produced with SCMs," *SP-308, American Concrete Institute, Farmington Hills, MI, 2016*, pp. 1-16.
53. Suraneni, P.; Jafari Azad, V.; Isgor, O. B.; and Weiss, W. J., "Deicing Salts and Durability of Concrete Pavements and Joints: Mitigating Calcium Oxychloride Formation," *Concrete International*, V. 38, No. 4, Apr. 2016, pp. 48-54.
54. Kim, J. J.; Foley, E. M.; and Reda Taha, M. M., "Nano-mechanical Characterization of Synthetic Calcium-Silicate-Hydrate (C-S-H) with Varying CaO/SiO₂ Mixture Ratios," *Cement and Concrete Composites*, V. 36, 2013, pp. 65-70. doi: 10.1016/j.cemconcomp.2012.10.001
55. Khan, S. U.; Nuruddin, M. F.; Ayub, T.; and Shafiq, N., "Effects of Different Mineral Admixtures on the Properties of Fresh Concrete," *The Scientific World Journal*, V. 2014, 2014, p. 986567 doi: 10.1155/2014/986567
56. Durdziński, P. T.; Ben Haha, M.; Bernal, S. A.; De Belie, N.; Gruyaert, E.; Lothenbach, B.; Menéndez Méndez, E.; Provis, J. L.; Schöler, A.; Stabler, C.; Tan, Z.; Villagrán Zaccardi, Y.; Vollpracht, A.; Winnefeld, F.; Zajac, M.; and Scrivener, K. L., "Outcomes of the RILEM Round Robin on Degree of Reaction of Slag and Fly Ash in Blended Cements," *Materials and Structures*, V. 50, No. 2, 2017, p. 135 doi: 10.1617/s11527-017-1002-1
57. Haha, M. B.; De Weerd, K.; and Lothenbach, B., "Quantification of the Degree of Reaction of Fly Ash," *Cement and Concrete Research*, V. 40, No. 11, 2010, pp. 1620-1629. doi: 10.1016/j.cemconres.2010.07.004
58. ASTM C618-17a, "Standard Specification for Coal Fly Ash and Raw or Calcined Natural Pozzolan for Use in Concrete," ASTM International, West Conshohocken, PA, 2017, 5 pp.
59. Pour-Ghaz, M., *Detecting Damage in Concrete Using Electrical Methods and Assessing Moisture Movement in Cracked Concrete*, Purdue University, West Lafayette, IN, 2011.
60. Singh, L. P.; Goel, A.; Bhattacharyya, S. K.; and Mishra, G., "Quantification of Hydration Products in Cementitious Materials Incorporating Silica Nanoparticles," *Frontiers of Structural and Civil Engineering*, V. 10, No. 2, 2015, pp. 162-167. doi: 10.1007/s11709-015-0315-9
61. De la Varga, I.; Castro, J.; Bentz, D.; Zunino, F.; and Weiss, W., "Evaluating the Hydration of High Volume Fly Ash Mixtures Using Chemically Inert Fillers," *Construction and Building Materials*, V. 161, Feb. 2018, pp. 221-228.
62. Kunther, W.; Ferreira, S.; and Skibsted, J., "Influence of the Ca/Si Ratio on the Compressive Strength of Cementitious Calcium-Silicate-Hydrate Binders," *Journal of Materials Chemistry. A, Materials for Energy and Sustainability*, V. 5, No. 33, 2017, pp. 17401-17412. doi: 10.1039/C7TA06104H
63. Hong, S.-Y., and Glasser, F. P., "Alkali Binding in Cement Pastes Part I. The C-S-H Phase," *Cement and Concrete Research*, V. 29, 1999.
64. Vidmer, A.; Sclauzero, G.; and Pasquarello, A., "Infrared Spectra of Jennite and Tobermorite from First-Principles," *Cement and Concrete Research*, V. 60, 2014, pp. 11-23. doi: 10.1016/j.cemconres.2014.03.004
65. Vollpracht, A.; Lothenbach, B.; Snellings, R.; and Haufe, J., "The Pore Solution of Blended Cements: A Review," *Materials and Structures*, V. 49, No. 8, 2015, pp. 3341-3367. doi: 10.1617/s11527-015-0724-1
66. Bouasker, M.; Khalifa, N. E. H.; Mounanga, P.; and Ben Kahla, N., "Early-Age Deformation and Autogenous Cracking Risk of Slag-Limestone Filler-Cement Blended Binders," *Construction and Building Materials*, V. 55, 2014, pp. 158-167. doi: 10.1016/j.conbuildmat.2014.01.037
67. Hong, S.-Y., and Glasser, F. P., "Alkali Sorption by C-S-H and C-A-S-H Gels Part II. Role of Alumina," *Cement and Concrete Research*, V. 32, No. 7, 2002, pp. 1101-1111. doi: 10.1016/S0008-8846(02)00753-6